Quaternary Science Reviews 30 (2011) 1988–2001

Contents lists available at ScienceDirect

Quaternary Science Reviews

journal homepage: www.elsevier.com/locate/quascirev

Palaeoglaciology of Bayan Har Shan, NE Tibetan Plateau: exposure ages reveal a missing LGM expansion

Jakob Heyman [a,b,*], Arjen P. Stroeven [b], Marc W. Caffee [c], Clas Hättestrand [b], Jonathan M. Harbor [a], Yingkui Li [d], Helena Alexanderson [b,e], Liping Zhou [f], Alun Hubbard [g]

[a] Department of Earth and Atmospheric Sciences, Purdue University, West Lafayette, IN 47907-1397, USA
[b] Department of Physical Geography and Quaternary Geology, Stockholm University, 10691 Stockholm, Sweden
[c] Department of Physics, Purdue Rare Isotope Measurement Laboratory, Purdue University, West Lafayette, IN 47907 1397, USA
[d] Department of Geography, University of Tennessee, Knoxville, TN 37996, USA
[e] Department of Earth and Ecosystem Sciences, Lund University, 22362 Lund, Sweden
[f] Department of Geography, Peking University, Beijing 100871, China
[g] Institute of Geography and Earth Sciences, Aberystwyth University, Aberystwyth SY23 3DB, UK

ARTICLE INFO

Article history:
Received 6 January 2011
Received in revised form
3 May 2011
Accepted 5 May 2011
Available online 31 May 2011

Keywords:
Tibetan plateau
Palaeoglaciology
Bayan Har
Exposure dating

ABSTRACT

The Bayan Har Shan, a prominent upland area in the northeastern sector of the Tibetan Plateau, hosts an extensive glacial geological record. To reconstruct its palaeoglaciology we have determined ^{10}Be exposure ages based on 67 samples from boulders, surface pebbles, and sediment sections in conjunction with studies of the glacial geology (remote sensing and field studies) and numerical glacier modelling. Exposure ages from moraines and glacial sediments in Bayan Har Shan range from 3 ka to 129 ka, with a large disparity in exposure ages for individual sites and within the recognised four morphostratigraphical groups. The exposure age disparity cannot be explained by differences in inheritance without using unrealistic assumptions but it can be explained by differences in post-depositional shielding which produces exposure ages younger than the deglaciation age. We present a palaeoglaciological time-slice reconstruction in which the most restricted glaciation, with glaciers less than 10 km long, occurred before 40–65 ka. More extensive glaciations occurred before 60–100 ka and 95–165 ka. Maximum glaciation is poorly constrained but probably even older. The Bayan Har Shan exposure age dataset indicates that glaciers on the northeastern Tibetan Plateau have remained surprisingly restricted for at least 40 ka, including the global last glacial maximum (LGM). This case of a missing LGM is further supported by high-resolution glacier modelling experiments.

1. Introduction

The Tibetan Plateau is a unique topographic feature exerting a major impact on regional and global climate (Raymo and Ruddiman, 1992; An et al., 2001) and it hosts a large part of the present-day glaciers outside the polar areas (Dyurgerov and Meier, 2005). Constraining the chronology of past glacier variations on the Tibetan Plateau can help resolving climate dynamics on a global scale (e.g. influence of Northern Hemisphere ice sheet expansions) and on a regional scale (e.g. monsoon influence). Glacier extents on the Tibetan Plateau have been dated using luminescence (e.g. Richards, 2000), radiocarbon (e.g. Yi et al., 2007), and cosmogenic exposure techniques (e.g. Owen et al., 2008). Despite important advances towards a glacial chronology by dating a large number of boulders using the cosmogenic exposure technique (e.g. Owen et al., 2008; Heyman et al., 2011), important knowledge gaps remain, particularly for glaciations pre-dating the global last glacial maximum (LGM; Clark et al., 2009).

Reconstructions of Tibetan Plateau palaeoglaciers for the LGM range from a plateau-wide ice sheet to limited mountain glaciers. Kuhle (2004 and references there-in) has argued that the entire plateau was covered by an extensive ice sheet (with an extent similar to that of the current Greenland ice sheet), whereas a vast quantity of evidence regarding Tibetan Plateau glaciations is consistent with a limited glacier expansion with glaciers restricted to the highest mountain areas (e.g. Derbyshire et al., 1991; Rutter, 1995; Zheng and Rutter, 1998; Schäfer et al., 2002; Zhou et al., 2004; Lehmkuhl and Owen, 2005; Owen et al., 2005, 2008; Heyman et al., 2009).

* Corresponding author. Department of Earth and Atmospheric Sciences, Purdue University, West Lafayette, IN 47907-1397, USA.
E-mail address: heyman@purdue.edu (J. Heyman).

0277-3791/$ – see front matter © 2011 Elsevier Ltd. All rights reserved.
doi:10.1016/j.quascirev.2011.05.002

Here we present ^{10}Be exposure ages from 67 samples from glacial deposits in the Bayan Har Shan, northeastern Tibetan Plateau, collected during three field seasons 2005–2007. The aim of the study was to constrain the timing of glaciation and to present a palaeoglaciological time-slice reconstruction suitable as target for glacial modelling. We have dated glacially transported boulders, aggregated samples of surface cobbles, and sediment section depth profiles. In doing so, we furthermore evaluate the merits of dating three different cosmogenic exposure sample types. The ^{10}Be exposure ages in conjunction with geomorphological mapping and stratigraphical evidence allow us to reconstruct the extent of past glaciers and propose a chronological framework.

2. Study area and previous studies

Bayan Har Shan is part of the northeastern sector of the Tibetan Plateau and encompasses the headwaters of the Huang He (Yellow River) in the north and the Chang Jiang (Yangtze River) in the southwest (Fig. 1). It is situated in a region where the high-altitude low-relief plateau intersects with a lower-altitude and higher-relief landscape caused by river incision (Stroeven et al., 2009). The central Bayan Har Shan, around which our ^{10}Be exposure age work is concentrated, is a low-relief mountain range summiting at c. 5200 m a.s.l. and rising c. 700–1200 m above the surrounding 4000–4500 m a.s.l. gentle plateau surface. The geology is dominated by sedimentary bedrock with granite intrusions in the centre of several mountain areas, including central Bayan Har Shan (Huang et al., 2004). Most of the relatively flat landscape is covered by sediments of glacial, glaciofluvial and fluvial origin (Heyman et al., 2009; Stroeven et al., 2009). Wide and rather indistinct glacial troughs, up to 60 km long, and U-shaped glacial valleys radiate outwards from the highest mountains (Fig. 2; Heyman et al., 2008; Stroeven et al., 2009). The glacial valleys contain several moraine ridges, extensive areas of hummocky terrain of glacial origin, and meltwater channels (Heyman et al., 2008, 2009). The moraine ridges are generally indistinct in the field but have clear surface expression on satellite imagery.

The glacial history of the Bayan Har range has been investigated in a number of studies, in which different extents of former glaciers have been proposed. Li et al. (1991), in their "Quaternary glacial distribution map for the Tibetan Plateau", presented two alternative views: glaciers restricted to the highest mountains and a regional-scale ice sheet – the Huang He ice sheet – centred on Bayan Har Shan. Zhou and Li (1998) presented a four-stage glacial reconstruction for the Bayan Har Shan based on mapped glacial landforms and sediments. The oldest Huang He ice sheet stage, during marine isotope stage (MIS)-16, was followed by a slightly smaller ice mass that existed during the Yematan glaciation of

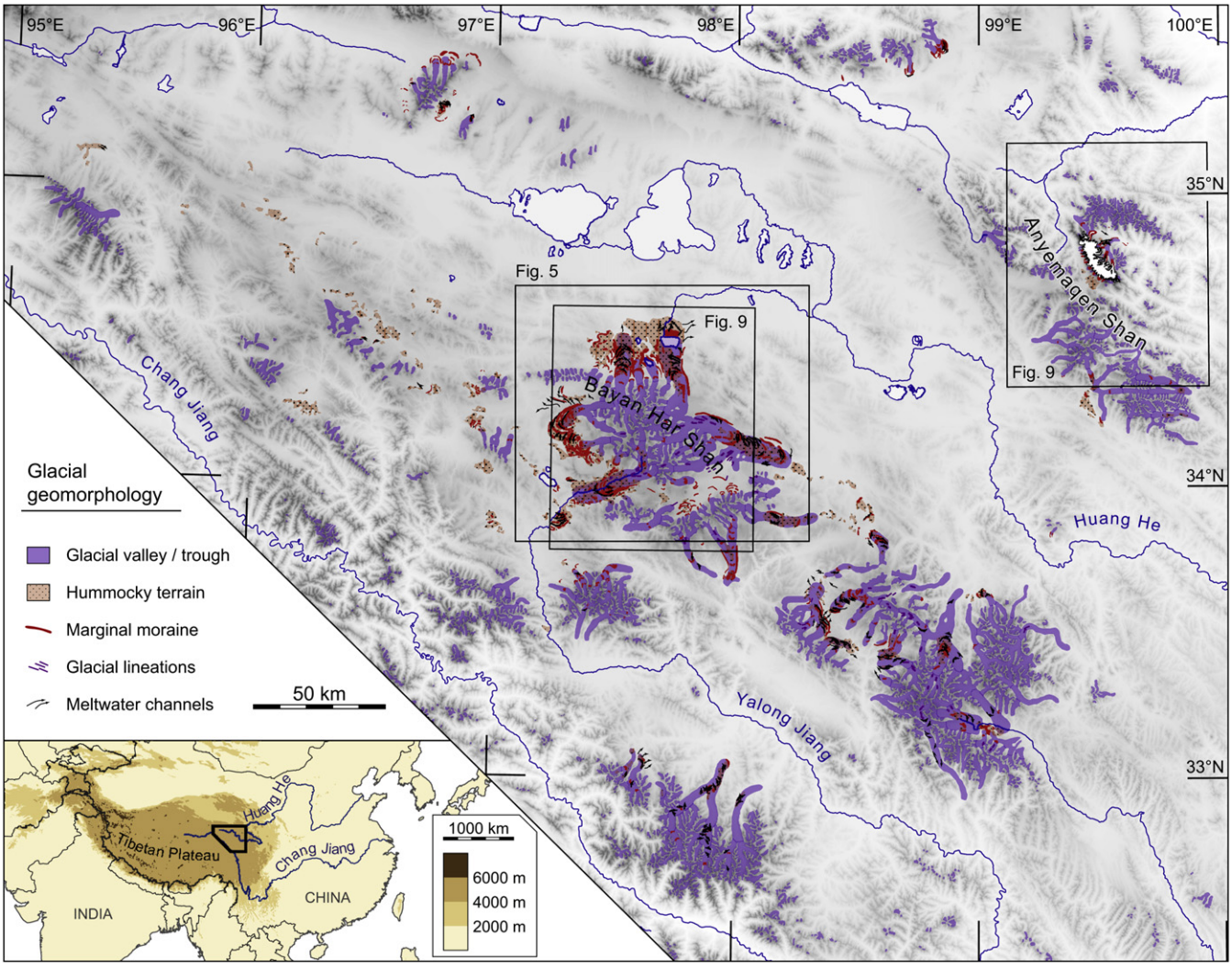

Fig. 1. Glacial geomorphology of Bayan Har Shan (Heyman et al., 2008) and the location of the study area in the northeastern corner of the Tibetan Plateau (inset map). The black boxes depict the locations of Figs. 5 and 9.

Fig. 2. Landscape photos from glacially eroded valleys/troughs in the central Bayan Har Shan study area. See Fig. 5 for locations. (a) Looking up-valley from site D into the highest part of central Bayan Har Shan. (b) Looking up-valley from site F in the Qingshuihe Valley. A road is visible in the photo. (c) Looking down-valley from site G in the Chalaping Valley. Sample TB-06-46 was collected from the boulder.

MIS-6, and two additional stages, the Galala stage and the Bayan Har stage, with more restricted glaciers during the last glacial cycle. The presence of a regional-scale ice sheet has subsequently been opposed based on the evidence that glacial landforms are restricted to the elevated mountain areas and because glacial sediments are absent on lower-lying plateau areas surrounding the mountain massifs (Lehmkuhl et al., 1998; Zheng and Rutter, 1998; Heyman et al., 2008, 2009; Stroeven et al., 2009). Currently the only chronological constraints from the Bayan Har are undocumented radiocarbon (50 000 BP) and thermoluminescence (133 ± 23 ka) dates from sediments assumed to cover glacial deposits of the Yematan glaciation (Zhou and Li, 1998). Thus, to define the timing of former glacial advances additional chronological constraints from glacial deposits are required.

Within the study area additional age constraints come from the Anyemaqen Shan, 180 km northeast of the Bayan Har Shan (Fig. 1). Owen et al. (2003a) presented cosmogenic exposure and optically stimulated luminescence dates, from sites within 12 km from present-day glaciers in the Anyemaqen Shan, ranging from 2 ka to 49 ka (CRONUS Lm scaling; Heyman et al., 2011). They suggested that the glaciers advanced during MIS-3, MIS-2, and the early Holocene. Cosmogenic exposure ages of predominantly glacially transported boulders have also been presented from a large number of other sites on the Tibetan Plateau (Owen et al., 2008; Heyman et al., 2011) and they range up to 562 ka (CRONUS Lm scaling; Heyman et al., 2011).

3. Methods

3.1. Sampling for cosmogenic exposure dating

Quartz-rich samples for ^{10}Be exposure age dating were collected from glacial boulders, surface pebbles and sediment section profiles (Fig. 3). Most samples were collected from moraine ridges. We collected 1–5 cm thick cosmogenic samples from the top surfaces of the largest boulders close to the crest of moraine ridges, using hammer and chisel, and measured the boulder size. Aggregated samples of 20–50 surface pebbles with *a*-axes of 1–5 cm were collected from most locations. We sampled four sediment sections (154–260 cm high), collecting aggregated pebbles or individual quartz-rich cobbles from three to five different horizons of recently cleared road pit sections. Altitude and location were recorded using a hand-held GPS and topographic shielding was measured with a compass and clinometer. The rationale behind dating multiple sample types was that they have potentially experienced different exposure histories and that combining them may facilitate robust exposure age interpretations. See Supplementary material for photographs of the samples.

3.2. Geochemistry and exposure age calculations

Sample crushing and sieving to 250–500 μm was done at Peking University or Purdue University. All sample geochemistry was carried out at Purdue Rare Isotope Measurement Laboratory (PRIME Lab) following a modified version of the preparations described in Kohl and Nishiizumi (1992) for quartz separation, and followed by Be carrier addition, ion exchange chromatography, and conversion to beryllium oxide. Ratios of ^{10}Be/^{9}Be were measured by accelerator mass spectrometry at PRIME Lab with normalization to the ^{10}Be standard ICN-01-5-3 with either the previous (6.990×10^{-12}) or the revised (6.320×10^{-12}) ^{10}Be/^{9}Be ratio (Nishiizumi et al., 2007). Exposure ages were calculated using the CRONUS online calculator (version 2.2, constants file 2.2.1; Balco et al., 2008) using a ^{10}Be half-life of 1.387 Ma (Chmeleff et al., 2010; Korschinek et al., 2010), taking account of the ^{10}Be standardization, and assuming an absence of inheritance and

Fig. 3. Types of samples collected for ^{10}Be exposure dating. (a) Boulder sample (TB-07-92). (b) Surface pebble sample (TB-07-30). (c) Sediment section profile samples (location J).

post-depositional surface erosion, a density of 2.7 g/cm^3, and assuming continuous post-depositional exposure to the full surface flux of cosmic rays (cf. Heyman et al., 2011). Exposure ages in this paper are the CRONUS Lm exposure ages based on the production rate scaling of Lal (1991) and Stone (2000) with palaeo-magnetic corrections following Nishiizumi et al. (1989).

To calculate exposure ages based on the sediment section ^{10}Be data we assume that the ^{10}Be concentration N (atoms g^{-1}) varies with depth beneath the surface similar to the depth-dependent ^{10}Be production rate according to Lal (1991):

$$N(d) = N(0)e^{-\rho d/\Lambda} \quad (1)$$

where d is depth beneath the surface (cm), ρ is sediment density (g cm^{-3}), and Λ is the attenuation length (g cm^{-2}). We fit the exponential function (Eq. 1) to the measured ^{10}Be data using the Nelder and Mead (1965) simplex method with Λ set to 160 g cm^{-2} (cf. Gosse and Phillips, 2001; Balco et al., 2008) and thus derive the surface ^{10}Be concentration $N(0)$ and the sediment density ρ. We use $N(0)$ to calculate a sediment section exposure age assuming that the sediment section has experienced no disturbance and that the surface has remained the same since deposition/deglaciation. To evaluate the geological uncertainty of the sediment section surface exposure age we calculate another two exposure ages for idealised disturbance scenarios. In all sediment sections, the top unit is fine-grained and of proposed aeolian origin (Heyman et al., 2009). Assuming, in one scenario, that the fine-grained top unit is a feature that has recently been deposited, we employ the ^{10}Be concentration at the lower boundary of the top unit to calculate a minimum estimate of the surface exposure age. Assuming, alternatively, that the top unit was formerly thicker and that 30 cm was recently removed, we use the ^{10}Be concentration of the fitted curves 30 cm above the surface to calculate a maximum estimate of the surface exposure age. The idealised scenarios represent simplified geological histories, but they yield quantitative data on the effect of surface alterations.

Our approach to derive surface exposure ages may introduce errors of several sources (cf. Goehring et al., 2010; Hidy et al., 2010). Production of ^{10}Be due to muon interaction (Granger and Smith, 2000) is not taken into account, the sediment density is assumed equal throughout the section and over time (cf. Rodés et al., 2011), and the section ^{10}Be concentrations are assumed resulting from a time-constant production rate (cf. Nishiizumi et al., 1989). However, these errors are minor compared to the potential errors introduced by the geological uncertainties and a simple exponential fit is therefore justified.

3.3. Morphostratigraphy of the sample sites

To enable a palaeoglaciological reconstruction with the exposure ages as chronological constraints, we have grouped our evidence in morphostratigraphic units. The grouping is based on the mapped glacial geomorphology (Heyman et al., 2008, 2009), and, in an effort to remain objective, parent glacier lowest altitude was matched against ice flow-line length for each of the sampling sites (Fig. 4; cf. Barr, 2009).

3.4. Three-dimensional glacier modelling

As a test of the climate forcing required to initiate glaciation in the Bayan Har Shan and expand the glaciers of the Anyemaqen Shan, a high-resolution mass balance and three-dimensional numerical ice flow model was applied to these two areas. Input data consisted of the SRTM topography (Jarvis et al., 2008), resampled to a resolution of 15 s (c. 380 × 460 m), and mean monthly precipitation and temperature (Hijmans et al., 2005; modified to the topography with a lapse rate of −0.006 K m^{-1}), both with original resolutions of 30 s. A positive degree day model with a degree day factor of 4.1 mm d^{-1} K^{-1} (cf. Braithwaite, 2008) yields the mass balance parameterization and a higher order ice flow model (Hubbard et al., 1998; Hubbard, 1999, 2000) yields the glacier outline. Key ice flow model parameters are presented in Table 1. The ice flow and sliding parameters were chosen to produce glacier tongues of plausible outline for the two areas. The model was run to steady state (3000–10000 years) with the present-day climate and with perturbations of temperature (−1.5 K and −3 K) and precipitation (300% and 1200%).

4. Site descriptions

An aggregated sample of surface pebbles was collected from an ice-cored moraine of the Weigele Dangxiong Glacier at the Anyemaqen ice field (Fig. 1), within 100 m from the clean ice glacier surface. This sample was collected as a test for cosmogenic inheritance due to prior exposure.

We collected 66 samples from 15 locations in and around the central Bayan Har Shan (Figs. 4 and 5). Sampling was performed in valleys opening towards the north (Galala Valley), east (Chalaping Valley) and south (Qingshuihe Valley), and north of the Yeniugou Mountains. Boulders occurred infrequently and were relatively small, however, with the highest boulder frequency occurring in the Galala area north of the granite bedrock source (Fig. 5; cf. Heyman et al., 2009).

Locations A–D are situated closest to the central massif and thus represent the morphostratigraphically youngest unit (BH-1). The sampling sites are located on subtle moraine ridges (cf. Fig. 6) formed by glaciers 4–8 km long and extending down to 4740–4540 m a.s.l. Unit BH-1 is morphostratigraphically distinguished from the other units by the short lengths of the parent glaciers (Fig. 4). In total, eight boulder samples, four pebble

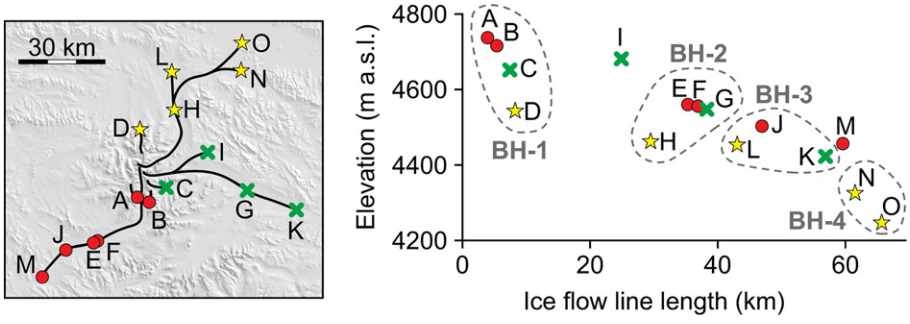

Fig. 4. Location of the sites with lowest elevation and inferred ice flow line lengths for the parent glaciers (cf. Barr, 2009) and morphostratigraphic groups BH-1 to BH-4.

Table 1
Key parameters for the mass balance and ice flow model.

Parameter	Central Bayan Har Shan	Anyemaqen Shan
Domain size	200 × 200 grids	200 × 200 grids
Grid resolution (seconds)	15	15
Degree day factor (mm d^{-1} K^{-1})	4.1	4.1
Lapse rate (K m^{-1})	−0.006	−0.006
Flow parameter (s^{-1} kPa^{-3})	5.05×10^{-16}	5.05×10^{-17}
Sliding parameter	10^{-13}	7.5×10^{-16}
Time step (years)	0.05	0.01–0.05

samples, and three samples from the sediment section at C were collected from group BH-1.

Locations E–H are situated 29–38 km down-valley from the highest mountains (Figs. 4 and 5). The sampling sites for E and F are located on two nested moraine ridges 1.5 km apart in Qingshuihe Valley (Fig. 6). The outer moraine (E) forms a clear ridge outlining the location of a former glacier tongue in the valley. The sampling sites for G and H are located on a large moraine ridge in Chalaping Valley (Fig. 6) and on a subdued moraine ridge in Galala Valley, respectively. Locations E–H form the second youngest morphostratigraphic group, BH-2, with ice flow line lengths of 29–38 km and lowest glacier altitudes of 4560–4460 m a.s.l. In total, eleven boulder samples, three pebble samples, and five samples from the sediment section at F were collected from group BH-2.

Location I is situated c. 25 km away from the highest mountains on a shoulder north of Chalaping Valley (Figs. 4 and 5) at 4700 m a.s.l. Although location I occurs north of the lateral moraine connected with the frontal moraine at G, we do not exclude the possibility that it might have been ice covered when this moraine was formed. The lateral moraine south of location I might have formed time-transgressively later than the moraine ridge at G. However, because of these uncertainties, location I has been excluded from the morphostratigraphic groups. Two boulders were sampled at location I.

Locations J–L are situated 43–57 km down-valley from the mountain summits, and were formed by glaciers with lowest altitudes of 4500–4420 m a.s.l., and form the third youngest morphostratigraphic group, BH-3 (Figs. 4 and 5). Sampling sites at location J in Qingshuihe Valley occur c. 10 km down-valley of E. Mapped and photographed remnants of a latero-frontal moraine ridge occur on the southern side of the valley (and river). The samples at location J were collected from a till surface on the northern side of the valley/river, in a morphostratigraphic position corresponding to the moraine ridge remnants on the other side of the valley (see Fig. 6). The sampling sites of locations K and L occur on a large lateral moraine in Chalaping Valley, 19 km down-valley of

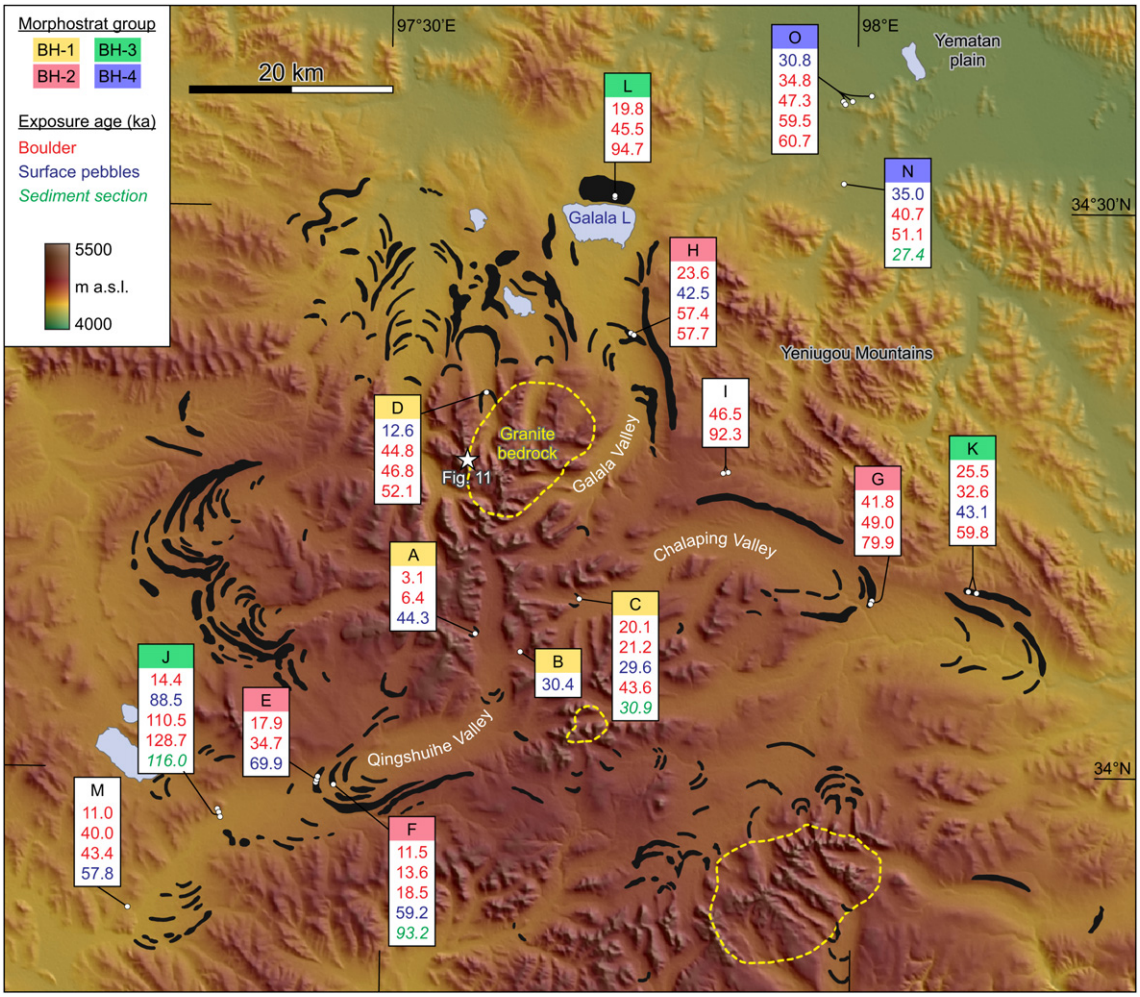

Fig. 5. Central Bayan Har Shan with marginal moraines (Heyman et al., 2008), granite bedrock areas mapped from Landsat ETM + satellite imagery (dashed lines; Heyman et al., 2009), exposure ages, morphostratigraphic groups of the sample sites, and location of the end moraine depicted in Fig. 11. See Table 2 and Supplementary material for exposure age data including uncertainties. See Fig. 1 for location of the depicted area.

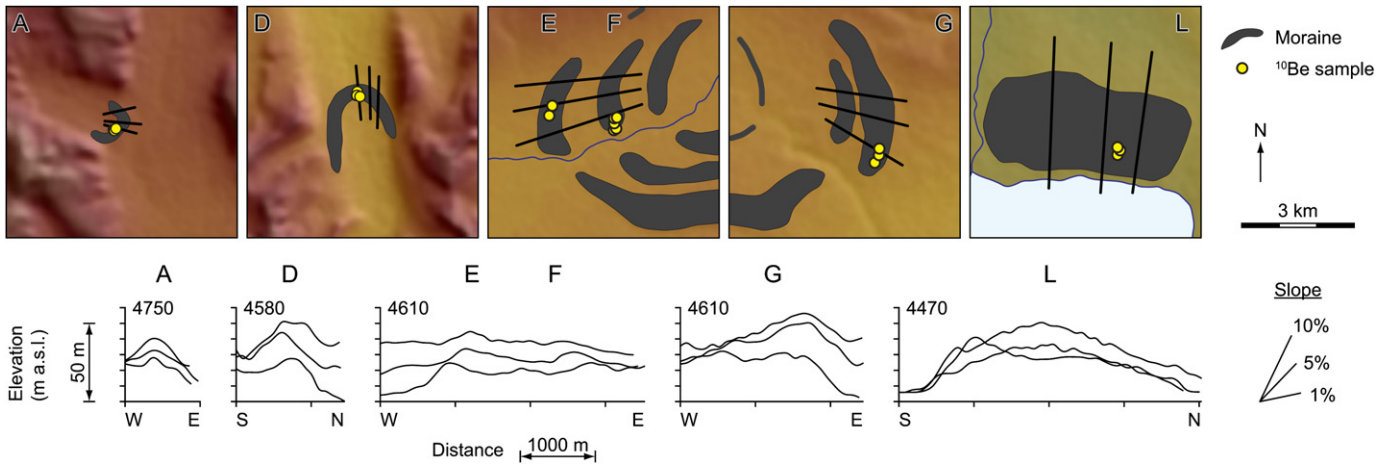

Fig. 6. Map and elevation profiles over moraine ridges from locations A, D, E, F, G and L. The elevation profiles illustrate that the moraine ridges are subtle features indicating that they may have experienced substantial degradation (cf. Putkonen et al., 2008). See Fig. 5 for location of the sites.

G, and on the large moraine impounding the Galala Lake (Fig. 6), 14 km down-valley of H, respectively. In total, nine boulder samples, two pebble samples, and three samples from the sediment section at J were collected from group BH-3.

Location M is situated 13 km down-valley of J in the lower reaches of Qingshuihe Valley, opposite to a group of subtle moraine ridges and meltwater channels (Figs. 4 and 5), at 4500 m a.s.l. Because of its down-valley position relative to J it represents a more extensive glacial phase. However, considering the geomorphology of the area, including the unclear outline of the moraine at location J, we do not exclude the possibility that both sites in fact belong to the same morphostratigraphic group, BH-3, where J then represents a deglacial stage. In consideration of these uncertainties, however, location M has not been assigned to a specific morphostratigraphic group. Three boulder samples and one pebble sample were collected at location M.

Locations N and O are situated c. 60 km northeast of the highest mountains in the Bayan Har Shan and at altitudes of 4350–4250 m a.s.l., north of the Yeniugou Mountains and at the southern margin of the Yematan plain, respectively (Fig. 5). The samples from location N were drawn from an elevated body of glaciofluvial sediments with scattered erratic granite boulders (Lehmkuhl et al., 1998; Heyman et al., 2009). Sample sites at location O occur at the break-in-slope between the flat Yematan plain (fluvial infill of the Huang He) and the foothills leading up to the Bayan Har Shan. The occurrence of scattered erratic granite boulders along the break-in-slope has been interpreted to indicate the minimum extent of an ice mass that formerly extended onto the Yematan plain, but the traces of which have been buried by post-glacial fluvial sediments (Zhou and Li, 1998; Heyman et al., 2009). Because locations N and O, in comparison to the others, occur at significantly lower elevations and at further distances from the central mountain area, where no large-scale glacial landforms have been mapped (Fig. 4; Heyman et al., 2008, 2009), we associate them with a separate morphostratigraphic group, BH-4. In total, six boulder samples, two pebble samples, and four samples from the sediment section at N were collected from group BH-4.

5. Results

5.1. ^{10}Be exposure ages

The derived exposure ages are presented in Table 2, Figs. 5,7, and 8, and Supplementary material (for the full dataset, including CRONUS calculator input and output). The dataset is characterized by significant exposure age disparity, both within morphostratigraphic groups and for individual locations. Sampled boulders have exposure ages ranging from 3.1 ± 0.4 ka to 128.7 ± 11.6 ka (Fig. 7). The Anyemaqen Shan pebble sample (TB-07-06) has an exposure age of 0.54 ± 0.07 ka and the central Bayan Har Shan pebble samples have exposure ages ranging from 12.6 ± 1.1 ka to 88.5 ± 7.8 ka. Three sediment section profiles (locations F, J, N) have ^{10}Be concentrations decreasing with depth whereas one sediment section profile (C) has ^{10}Be concentrations increasing with depth (Table 3; Fig. 8). Calculated exposure ages at location C are, therefore, based on the uppermost (youngest exposure age) sample only with an assumed sediment density of 1.8 g cm^{-3} similar to sections J and N. The sediment sections have surface exposure ages ranging from 27.4 ka to 116.0 ka and the idealised disturbance scenarios yield minimum exposure estimates 23%–39% younger and maximum exposure estimates 32%–43% older (Figs. 7 and 8). Table 4 presents the exposure age data for boulders, pebbles, and sediment sections organised by morphostratigraphic group.

5.2. Glacier modelling

Under the present-day climate regime (0 K perturbation and 100% precipitation) a realistic accumulation area (area of positive mass balance) and a glacier extent c. 60% larger than currently present are produced for the Anyemaqen ice field (Fig. 9). The mismatch between modelled and current glacier extent can be explained by the fact that the model starts growing ice on the SRTM representation of the present-day landscape, i.e. grows an ice body on top of the topography including the present-day glacier surface. Thus, in a qualitative sense, the Anyemaqen Shan model results for present-day conditions lend credibility to the employed mass balance and ice flow approach. To form small glaciers on the central Bayan Har Shan domain, the temperature needs to be depressed by 3 K (using present-day precipitation) or precipitation increased by 1200% (using present-day temperature). Applying the 3 K or 1200% climate perturbations to the Anyemaqen Shan area yields an ice mass far more extensive than can be motivated from mapped glacial landforms in the area (Wang, 1987; Owen et al., 2003a; Heyman et al., 2008). The higher sliding parameter used for the central Bayan Har domain (Table 1) facilitates initial glacier expansion. Using the lower Anyemaqen Shan sliding parameter for both domains would therefore increase the difference between the climate perturbations initiating glacier growth.

Table 2
Sample and exposure age data for the boulders, surface pebbles, and the three top unit emplacement scenarios for each sediment section.

Sample	Location	Boulder size l/w/h (cm)	Latitude (DD)	Longitude (DD)	Elevation (m a.s.l.)	Sample thickness (cm)	^{10}Be conc[a] (atoms g^{-1})	^{10}Be standardization[b]	Exposure age[c] (ka)
TB-07-06	Anyemaqen	Pebbles	34.87056	99.46533	4578	2	34939 ± 3382	07KNSTD	0.54 ± 0.07
TB-07-67	A	Pebbles	34.12367	97.59736	4724	2	3901533 ± 60878	07KNSTD	44.3 ± 3.8
TB-07-68	A	110/40/35	34.12322	97.59692	4723	2	492027 ± 27372	07KNSTD	6.4 ± 0.6
TB-07-69	A	110/50/40	34.12339	97.59664	4722	4	218880 ± 23547	07KNSTD	3.1 ± 0.4
TB-05-051	B	Pebbles	34.10817	97.64593	4780	2	2863533 ± 67520	KNSTD	30.4 ± 2.7
TB-07-22	C	60/30/15	34.15583	97.70839	4655	3	3683115 ± 57674	07KNSTD	43.6 ± 3.8
TB-07-23	C	45/25/11	34.15597	97.70864	4657	3	1541858 ± 55658	07KNSTD	20.1 ± 1.9
TB-07-24	C	70/40/15	34.15611	97.70842	4656	3	1636423 ± 53208	07KNSTD	21.2 ± 1.9
TB-07-25	C	Pebbles	34.15606	97.70853	4657	2	2375016 ± 95354	07KNSTD	29.6 ± 2.8
C-old	C	Section	34.15442	97.70806	4653	–	3546843[d]	07KNSTD	41.3 ± 3.5
C-surface	C	Section	34.15442	97.70806	4653	–	2530857[d]	07KNSTD	30.9 ± 2.6
C-young	C	Section	34.15442	97.70806	4653	–	1846991[d]	07KNSTD	23.2 ± 2.0
TB-07-92	D	120/100/40	34.33706	97.60703	4557	2	4218885 ± 42653	07KNSTD	52.1 ± 4.5
TB-07-93	D	230/160/40	34.33731	97.60611	4546	3	3607728 ± 63056	07KNSTD	44.8 ± 3.9
TB-07-94	D	340/240/60	34.33822	97.60622	4553	3	3785634 ± 49081	07KNSTD	46.8 ± 4.0
TB-07-95	D	Pebbles	34.33731	97.60589	4556	2	908979 ± 16733	07KNSTD	12.6 ± 1.1
TB-06-05	E	185/110/60	33.99186	97.43047	4593	4	2698702 ± 120402	07KNSTD	34.7 ± 3.3
TB-06-07	E	90/70/30	33.98956	97.42967	4590	5	1295018 ± 45804	07KNSTD	17.9 ± 1.6
TB-07-30	E	Pebbles	33.99192	97.43050	4589	2	5650626 ± 223112	07KNSTD	69.9 ± 6.6
TB-05-048	F	100/60/25	33.98931	97.44923	4576	1	1095537 ± 60276	KNSTD	13.6 ± 1.4
TB-05-049	F	120/100/100	33.98667	97.44905	4573	1	926260 ± 25214	KNSTD	11.5 ± 1.0
TB-05-050	F	120/80/50	33.98618	97.44835	4576	1	1521073 ± 58773	KNSTD	18.5 ± 1.7
TB-07-29	F	Pebbles	33.98789	97.44847	4574	2	4734788 ± 108725	07KNSTD	59.2 ± 5.3
F-old	F	Section	33.98911	97.44850	4584	–	10254259[d]	07KNSTD	122.8 ± 10.7
F-surface	F	Section	33.98911	97.44850	4584	–	7588951[d]	07KNSTD	93.2 ± 8.0
F-young	F	Section	33.98911	97.44850	4584	–	5905359[d]	07KNSTD	72.1 ± 6.2
TB-06-46	G	300/210/90	34.15353	98.01903	4573	3	3387690 ± 69642	07KNSTD	41.8 ± 3.7
TB-06-47	G	160/100/40	34.15539	98.02019	4583	4	3983409 ± 97952	07KNSTD	49.0 ± 4.4
TB-06-48	G	230/160/90	34.15697	98.02033	4592	3	6422910 ± 174573	07KNSTD	79.9 ± 7.2
TB-06-25	H	170/60/25	34.39111	97.76278	4516	4	4445208 ± 203908	07KNSTD	57.4 ± 5.6
TB-06-26	H	290/200/70	34.39153	97.75956	4509	2	1739523 ± 88529	07KNSTD	23.6 ± 2.3
TB-06-27	H	100/80/40	34.38983	97.76289	4518	4	4470809 ± 245943	07KNSTD	57.7 ± 5.9
TB-07-90	H	Pebbles	34.39239	97.76078	4512	2	3392391 ± 61553	07KNSTD	42.5 ± 3.7
TB-05-018	I	200/100/50	34.26853	97.85843	4716	1	4582101 ± 108155	KNSTD	46.5 ± 4.1
TB-05-019	I	300/200/100	34.26882	97.86542	4683	1	8702603 ± 205300	KNSTD	92.3 ± 8.3
TB-07-38	J	260/250/60	33.96175	97.32697	4536	2	1028089 ± 39038	07KNSTD	14.4 ± 1.3
TB-07-39	J	220/170/50	33.96436	97.32564	4556	2	8875375 ± 209714	07KNSTD	110.5 ± 9.9
TB-07-40	J	135/90/30	33.96444	97.32561	4557	3	10332818 ± 245352	07KNSTD	128.7 ± 11.6
TB-07-41	J	Pebbles	33.96478	97.32528	4560	2	6988376 ± 124618	07KNSTD	88.5 ± 7.8
J-old	J	Section	33.95764	97.32839	4515	–	13142531[d]	07KNSTD	166.2 ± 14.6
J-surface	J	Section	33.95764	97.32839	4515	–	9325764[d]	07KNSTD	116.0 ± 10.1
J-young	J	Section	33.95764	97.32839	4515	–	5574328[d]	07KNSTD	70.4 ± 6.0
TB-07-117	K	230/130/50	34.16397	98.13178	4648	5	2579480 ± 43928	07KNSTD	32.6 ± 2.8
TB-07-118	K	80/50/25	34.16431	98.13153	4646	4	1974653 ± 29779	07KNSTD	25.5 ± 2.2
TB-07-119	K	140/90/40	34.16547	98.12297	4638	4	4876360 ± 75567	07KNSTD	59.8 ± 5.2
TB-07-120	K	Pebbles	34.16419	98.13183	4646	2	3664705 ± 51235	07KNSTD	43.1 ± 3.7
TB-06-31	L	200/80/55	34.51156	97.74075	4456	4	3510188 ± 59762	07KNSTD	45.5 ± 4.0
TB-06-32	L	330/300/100	34.51344	97.74072	4451	4	7096037 ± 222592	07KNSTD	94.7 ± 8.7
TB-06-33	L	135/90/30	34.51272	97.74156	4453	3	1390923 ± 58892	07KNSTD	19.8 ± 1.9
TB-07-31	M	125/45/35	33.87681	97.23164	4500	3	3378996 ± 63091	07KNSTD	43.4 ± 3.8
TB-07-32	M	Pebbles	33.87692	97.23156	4501	2	4450103 ± 78004	07KNSTD	57.8 ± 5.0
TB-07-33	M	65/30/17	33.87703	97.23142	4498	3	3070453 ± 55724	07KNSTD	40.0 ± 3.5
TB-07-34	M	160/115/40	33.87586	97.23139	4493	3	753768 ± 38165	07KNSTD	11.0 ± 1.1
TB-06-16	N	130/90/30	34.52639	97.98719	4332	4	2917475 ± 54223	07KNSTD	40.7 ± 3.5
TB-06-17	N	150/110/40	34.52578	97.98753	4332	4	3689462 ± 133961	07KNSTD	51.1 ± 4.8
TB-07-13	N	Pebbles	34.52614	97.98694	4331	2	2472301 ± 112833	07KNSTD	35.0 ± 3.4
N-old	N	Section	34.52533	97.98503	4346	–	2728373[d]	07KNSTD	37.2 ± 3.2
N-surface	N	Section	34.52533	97.98503	4346	–	1929490[d]	07KNSTD	27.4 ± 2.3
N-young	N	Section	34.52533	97.98503	4346	–	1364524[d]	07KNSTD	19.9 ± 1.7
TB-06-01	O	110/80/65	34.59906	97.98464	4259	5	3290960 ± 114624	07KNSTD	47.3 ± 4.4
TB-06-02	O	72/56/40	34.59650	97.98686	4264	5	4127412 ± 104024	07KNSTD	60.7 ± 5.4
TB-06-37	O	90/70/23	34.59922	97.99461	4256	3	2353954 ± 94502	07KNSTD	34.8 ± 3.3
TB-07-12	O	Pebbles	34.59614	97.98625	4266	2	2082941 ± 88358	07KNSTD	30.8 ± 2.9
TB-07-125	O	135/70/55	34.60492	98.01506	4248	5	4020612 ± 137653	07KNSTD	59.5 ± 5.5

[a] See Supplementary dataset for complete ^{10}Be data including sample and carrier weight and sample and blank ^{10}Be/Be values.

[b] The CRONUS calculator standardization codes are used to indicate which isotope ratio was used for the ICN-01-5-3 ^{10}Be standard. Standardization 07KNSTD has a ^{10}Be/^{9}Be ratio of 6.320×10^{-12}, and standardization KNSTD has a ^{10}Be/^{9}Be ratio of 6.990×10^{-12} (Nishiizumi et al., 2007).

[c] Exposure ages have been calculated using the CRONUS online calculator (Balco et al., 2008) version 2.2 (constants file version 2.2.1) with a ^{10}Be half-life of 1.387 Ma (Chmeleff et al., 2010; Korschinek et al., 2010). Given exposure ages are from the CRONUS Lm production rate scaling scheme with external uncertainty. See Supplementary dataset for complete CRONUS input and output.

[d] The sediment section ^{10}Be concentrations are based on exponential curves fitted to the measured ^{10}Be data (Fig. 8) and do not include measurement uncertainty. See Table 3 for data on the individual samples of the sediment sections.

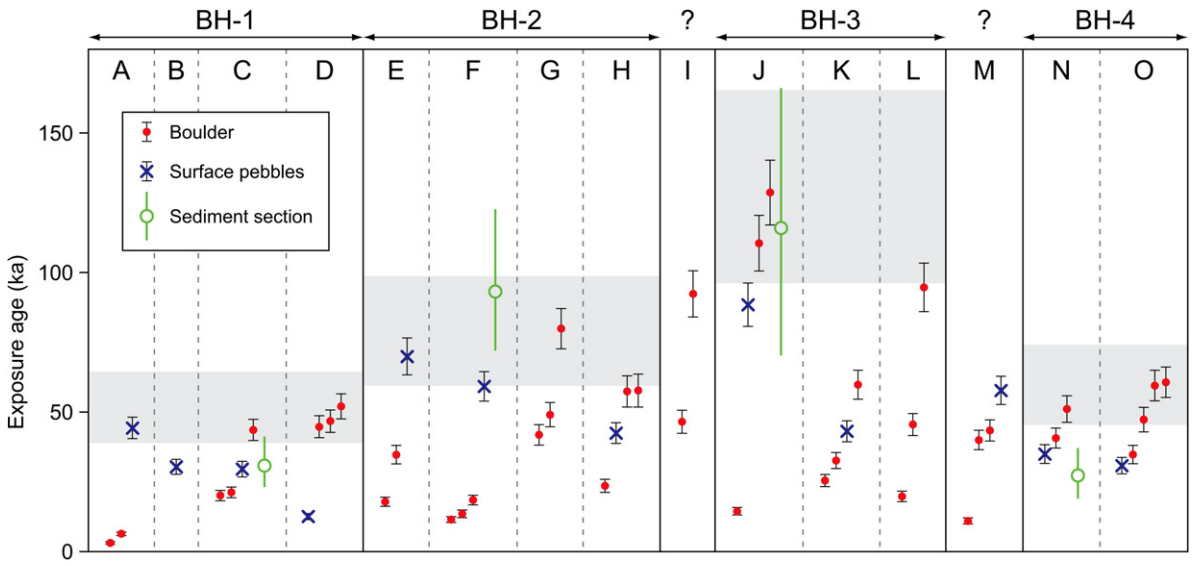

Fig. 7. Exposure ages (CRONUS Lm scaling with external uncertainty). For the sediment sections the surface exposure age is shown by the circle with the bars ending at the minimum and maximum estimates of the surface exposure age (cf. Fig. 8). The grey areas include the morphostratigraphic group (BH-1 to BH-4) oldest boulder exposure ages plus external uncertainties for all CRONUS production rate scaling schemes (cf. Supplementary Fig. 1). See Table 2 and Supplementary material for exposure age data.

6. Discussion

6.1. Exposure age interpretation

The young exposure age (0.54 ± 0.07 ka) of the surface pebble sample from the Weigele Dangxiong Glacier ice-cored moraine of the Anyemaqen Shan shows that this sample has experienced negligible inheritance due to prior exposure. This result is in accord with measured boulders from present-day glaciers and late Holocene moraines all over the world (Heyman et al., 2011).

Since production rate factors should not vary significantly for different samples of individual locations, geological factors need to be invoked to explain the wide spread in exposure ages. Similarly, assuming synchronous deposition of the samples within each morphostratigraphic group, geological factors are needed to explain the wide spread in exposure ages within the groups (Table 4; Fig. 7). Two geological factors of opposite character may generate exposure ages deviating from the actual age of deposition (Hallet and Putkonen, 1994; Putkonen and Swanson, 2003; Briner et al., 2005; Applegate et al., 2010; Heyman et al., 2011). First, exposure of a sample to cosmic rays prior to glacial entrainment and deposition yields inheritance, a cosmogenic nuclide concentration that is higher than expected and an exposure age older than deglaciation. Second, incomplete exposure due to partial shielding from cosmic rays subsequent to deposition, for example as a result of initial burial in sediments followed by later surface degradation and sample exhumation, yields a reduced cosmogenic nuclide concentration and an exposure age younger than deglaciation. In an attempt to remain objective, multiple working hypotheses (Chamberlin, 1890) are formulated to evaluate the explanatory power of the two end members: (i) the exposure age disparity is caused by prior exposure and exposure ages are maximum limiting deglaciation ages, or (ii) the exposure age disparity is caused by incomplete exposure and exposure ages are minimum limiting deglaciation ages.

6.1.1. Prior exposure

If the exposure age spread is caused solely by variations in prior exposure, the youngest exposure age of each site can be interpreted as a maximum limiting deglaciation age. The youngest exposure ages of the boulder and pebble samples for all locations fall between 3.1 ± 0.4 ka and 46.5 ± 4.1 ka. For the morphostratigraphic groups BH-1 to BH-4, the youngest exposure ages are 3.1 ± 0.4 ka, 11.5 ± 1.0 ka, 14.4 ± 1.3 ka, and 30.8 ± 2.9 ka (Tables 2 and 4; Fig. 7).

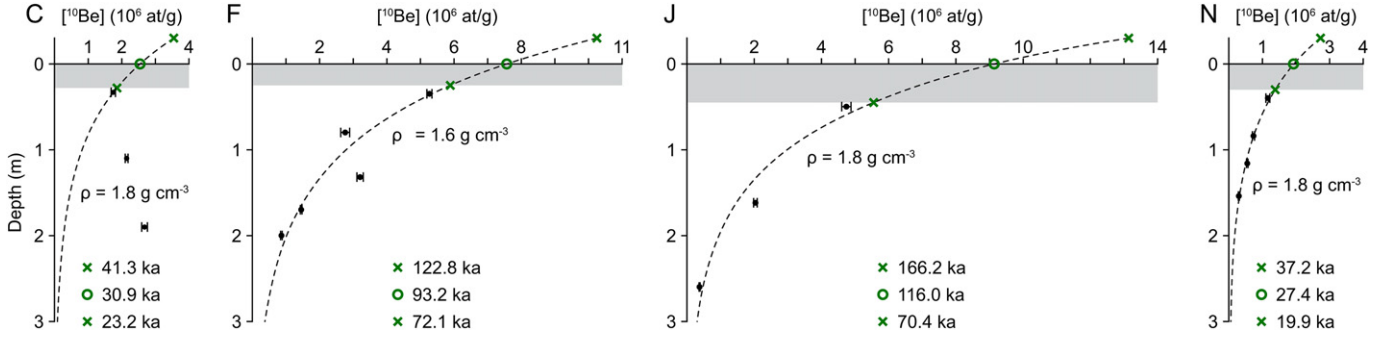

Fig. 8. Sediment section data and calculated exposure ages for the three top unit scenarios. The exponential curves of sections F, J, and N and their sediment densities ρ are derived from fitting Eq. (1) to the measured data. The exponential curve of section C represent Eq. (1) fitted to the uppermost sample ^{10}Be concentration only with ρ set to 1.8 g cm^{-3}. The grey areas represent the fine grained top unit. The sample data represent the ^{10}Be normalized to standardization 07KNSTD. See Tables 2 and 3, and Supplementary material, for ^{10}Be data including uncertainties.

Table 3
Sediment section sample data. See Table 2 for location data and sediment section surface exposure ages for three different top unit emplacement scenarios for each sediment section.

Sample	Sample depth (cm)	^{10}Be conc[a] (atoms g^{-1})	^{10}Be standardization[b]
Location C, top unit thickness: 28 cm			
TB-07-28	33	1745966 ± 62931	07KNSTD
TB-07-27	110	2142500 ± 39845	07KNSTD
TB-07-26	190	2677925 ± 83497	07KNSTD
Location F, top unit thickness: 25 cm			
TB-05-043	35	5832296 ± 83361	KNSTD
TB-05-044	80	3058921 ± 149099	KNSTD
TB-05-045	132	3551527 ± 102881	KNSTD
TB-05-046[c]	170	1462174 ± 25527	07KNSTD
TB-05-046[c]	170	1430574 ± 60566	07KNSTD
TB-05-047	200	871816 ± 22775	07KNSTD
Location J, top unit thickness: 45 cm			
TB-07-37	50	4747556 ± 138262	07KNSTD
TB-07-36	162	204086 ± 52653	07KNSTD
TB-07-35	260	378177 ± 17007	07KNSTD
Location N, top unit thickness: 30 cm			
TB-06-04–40 cm	40	1166057 ± 55626	07KNSTD
TB-06-04–84 cm	84	739577 ± 34145	07KNSTD
TB-06-04–116 cm	116	554690 ± 22528	07KNSTD
TB-06-04–154 cm	154	303800 ± 14407	07KNSTD

[a] See Supplementary dataset for complete ^{10}Be data including sample and carrier weight and sample and blank ^{10}Be/Be values.
[b] The CRONUS calculator standardization codes are used to indicate which isotope ratio was used for the ICN-01-5-3 ^{10}Be standard. Standardization 07KNSTD has a ^{10}Be/^{9}Be ratio of 6.320×10^{-12}, and standardization KNSTD has a ^{10}Be/^{9}Be ratio of 6.990×10^{-12} (Nishiizumi et al., 2007). For the section exposure age calculations (Fig. 8) the ^{10}Be measurements performed using standardization KNSTD were normalized to standardization 07KNSTD by a factor of 0.9042 similar to the CRONUS calculator and derived from Nishiizumi et al. (2007).
[c] Two measurements were performed for sample TB-05-046. For the exposure age calculations we used an uncertainty-weighted mean of the two ^{10}Be concentrations (see Supplementary material).

Assuming that youngest exposure ages represent correct deglaciation ages for each location, we can then quantify the amount of prior exposure by subtracting the youngest exposure age of a particular location from each exposure age at that location. When boulders are considered, this yields an average prior exposure (including one zero inheritance sample at each location) of 18.2 ka with 44% of the boulders being more than 10 ka older than the deglaciation age. When both boulder and pebble samples are considered, an average prior exposure of 22.4 ka results, with 53% of the samples being more than 10 ka older than the deglaciation age. To evaluate the significance of these potential average prior exposure values for the Bayan Har Shan, they can be compared with the amount of prior exposure that occurs for glacial boulders in the Northern Hemisphere palaeo-ice sheet areas (Heyman et al., 2011). Because the amount of inheritance in glacial boulders can be expected to be related to the amount of erosion that the ice sheet exerted on its bed, the analysis has been divided into separate analysis of relict areas (cf. Kleman, 1994; Kleman and Stroeven, 1997; Kleman and Hättestrand, 1999; Goodfellow, 2007), where erosion has been minimal and thus expected inheritance a maximum, and of glacially modified areas, where actively sliding ice has pervasively rearranged its underlying substrate. In relict areas 25% of the boulders ($n = 228$) have exposure ages more than 10 ka older than corresponding deglaciation ages, whereas in glacially modified areas only 4% of the boulders ($n = 403$) have exposure ages more than 10 ka older than corresponding deglaciation ages (Heyman et al., 2011). Because the Bayan Har Shan samples are likely derived from the glacially eroded U-shaped valleys (Heyman et al., 2008, 2009; Stroeven et al., 2009) the Bayan Har dataset should be preferentially compared to the glacially modified area palaeo-ice sheet dataset (4% > 10 ka older than deglaciation). Hence, to accept the prior exposure hypothesis for the explanation of exposure age spreads in the Bayan Har dataset, there also is a need to accept prior exposure of never before documented quantities.

An additional dataset to be considered in testing the prior exposure hypothesis, is the sediment section profiles ^{10}Be data (Table 3; Fig. 8). For sites C and N, the sediment section data could be explained with a prior exposure interpretation. The reversed order of ^{10}Be concentrations in the sediment section at location C may be a function of variations in prior exposure of the pebbles, and the extrapolated young surface exposure age of sediment section N may be interpreted to represent the correct deglaciation age with the boulders and pebbles from sites N and O all showing prior exposure. However, the ^{10}Be exposure ages of sediment sections F and J from Qingshuihe Valley, with decreasing ^{10}Be concentrations with depth below the surface and extrapolated surface exposure ages significantly older than the youngest exposure ages of boulders at these locations, is problematic for the prior exposure hypothesis. To reconcile the sediment sections F and J data with the prior exposure hypothesis, ice overriding these sediments and depositing younger boulders on top of the sediments would have to be inferred. Preservation of the sediments under glaciers depositing the younger boulders and surface pebbles also requires preservation of the moraine ridge at F. Preservation of moraine ridges under cold-based ice have been demonstrated for the Fennoscandian ice sheet but those moraines show traces of an overriding ice such as cross-cutting flutings and meltwater channels (Kleman, 1992; Fredin and Hättestrand, 2002; Fabel et al., 2006; Hättestrand et al., 2007). In contrast, the moraine ridges in Qingshuihe Valley show no signs of glacial overriding and the U-shaped valley, glacial trough, and its glacial lineations all signal processes of glacial erosion and landscape reworking rather than cold-based preservation. In summary, the extreme levels of prior exposure required to explain the spread in exposure ages and the sediment section ^{10}Be data from Qingshuihe Valley present immense problems for the prior exposure hypothesis which therefore fails to explain the observed spread in exposure ages of Bayan Har Shan.

6.1.2. Incomplete exposure

If the spread in exposure ages is caused by incomplete exposure due to post-depositional shielding, the oldest exposure age of each location represents a minimum limiting deglaciation age. The oldest exposure age of the boulders and surface pebbles fall

Table 4
Exposure ages of boulders, pebbles, and sediment sections, and the assigned minimum ages of glaciation for each of the four morphostratigraphic groups.

Morphostratigr-aphic group	Boulders			Pebbles			Sediment sections		Assigned minimum age range (ka)
	n	Age range (ka)	Mean age (ka)	n	Age range (ka)	Mean age (ka)	Age range (ka)	Surface age (ka)	
BH-1	8	3.1–52.1	29.7 ± 19.4	4	12.6–44.3	29.2 ± 13.0	23.2–41.3	30.9	40–65
BH-2	11	11.5–79.9	36.9 ± 22.2	3	42.5–69.9	57.2 ± 13.8	72.1–122.8	93.2	60–100
BH-3	9	14.4–128.7	59.1 ± 42.3	2	43.1–88.5	65.8 ± 32.1	70.4–166.2	116.0	95–165
BH-4	6	34.8–60.7	49.0 ± 10.2	2	30.8–35.0	32.9 ± 3.0	19.9–37.2	27.4	95–165

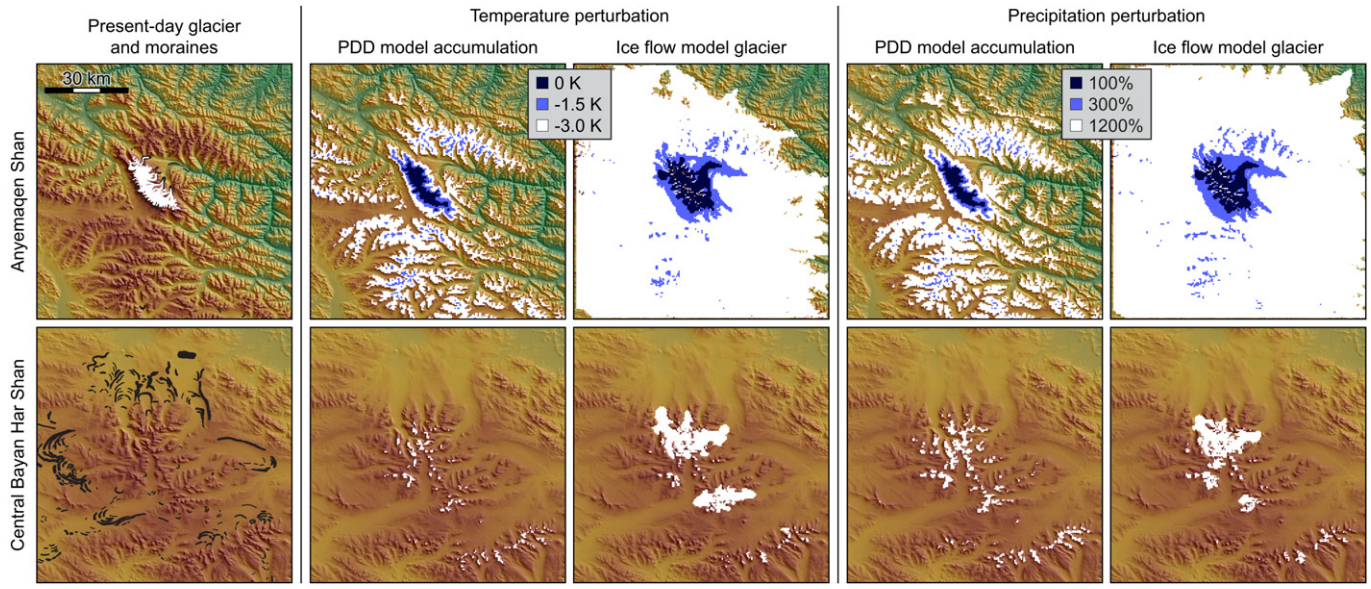

Fig. 9. Glacier model results, including positive degree day (PDD) accumulation area and glacier outline, for the central Bayan Har Shan and Anyemaqen Shan model domains. Model results are shown for present-day temperature and precipitation (0 K perturbation/100% precipitation), temperature perturbations of −1.5 K and −3.0 K (using present-day precipitation), and precipitation perturbations of 300% and 1200% (using present-day temperature). For the central Bayan Har Shan domain, small glaciers develop at a temperature perturbation of −3.0 K or a precipitation increase of 1200%. For the Anyemaqen Shan domain, a temperature perturbation of −1.5 K or a precipitation increase of 300% is enough to grow glaciers larger than indicated by the mapped moraines. A temperature decrease of 3 K or precipitation increase of 1200% result in massive ice growth, perhaps developing into an extensive ice cap or ice sheet if modelled on a larger domain. See Fig. 1 for location of the two domains.

between 30.4 ± 2.7 ka and 128.7 ± 11.6 ka for all locations, and the morphostratigraphic groups BH-1 to BH-4 have oldest exposure ages of 52.1 ± 4.5 ka, 79.9 ± 7.2 ka, 128.7 ± 11.6 ka, and 60.7 ± 5.4 ka (Tables 2 and 4; Fig. 7). If the post-depositional shielding hypothesis is correct, many samples have been shielded for extensive durations. Post-depositional shielding from cosmic rays can result from several processes such as snow cover, moraine degradation, boulder toppling, burial under post-glacial sediments, and surface erosion, all including some post-depositional duration with reduced cosmic ray bombardment of the sample. Moraine degradation, with potential sediment removal up to several tens of metres, has been frequently mentioned as a factor yielding exposure ages younger than deglaciation based on field data (e.g. Zreda et al., 1994; Briner et al., 2005; Zech et al., 2005) and numerical modelling (e.g. Hallet and Putkonen, 1994; Putkonen and Swanson, 2003; Putkonen et al., 2008; Applegate et al., 2010). Considering the subtle topography of the Bayan Har Shan moraines (Fig. 6), post-depositional moraine degradation is a credible process. Heyman et al. (2011) successfully formulated a simple landform degradation model in order to explain the important features of the spread in exposure ages for a comprehensive (n = 1361) glacial boulder exposure age dataset of the Tibetan Plateau. In addition to moraine degradation and sample exhumation, we hypothesize that boulder surface erosion and post-glacial sedimentary burial may have caused significant shielding. The infrequency of boulders in the Bayan Har Shan and the generally small size of the largest boulders may be interpreted as a result of surface erosion or post-glacial sedimentary burial. For locations N and O, positioned outside the area with mapped large-scale glacial landforms, burial under thicker aeolian sediments appears particularly plausible given the current presence of a fine-grained top unit of inferred aeolian origin. Because most of the samples from N and O were collected from gentle rises above the sedimentary plain, burial under fluvial sediments seems less likely. One alternative is burial under migrating sand dunes along the southern break-in-slope of the Yematan plain. Contemporary and relict sand dune fields are present north and east of locations N and O, indicating that past sand dunes may have covered the sites.

The ^{10}Be data of sediment sections at F, J, and N (Table 3; Fig. 8) are consistent with an incomplete exposure history for the locations. The relatively young ages of profile N can be explained by sediment burial and subsequent removal. The ^{10}Be data of profiles F and J in Qingshuihe Valley indicate limited inheritance in the glacial sediments and deglaciation ages significantly older than the youngest boulder ages. The ^{10}Be data of sediment section C is a problem for the incomplete exposure hypothesis. The reversed ^{10}Be concentrations can potentially be explained by either prior exposure of the glacial deposits or *in situ* mixing transporting previously exposed pebbles to deeper layers. Mixing could occur as a result of periglacial activity (cf. Cheng et al., 2005; Heyman et al., 2009), but the evidence from the other three sediment sections contradicts inferences for periglacial turnover to be an important process. There is also a possibility that section cleaning, removing slumped sediments to expose a fresh surface, has been unsuccessful. Given the range of possibilities, we acknowledge that the sediment section C pebble samples yield inconclusive evidence, and we refrain from drawing further conclusions.

The extreme difference between the boulder, surface pebbles, and sediment section exposure ages for locations A and F (Fig. 7) demand an explanation in light of the incomplete exposure hypothesis. Both sites display multiple young exposure ages and significantly older maximum exposure ages. The clustering of young exposure ages can be explained by an abrupt disruption of the shielding by, for example, an intensified short period of moraine degradation (cf. Schaefer et al., 2008). The boulders at location F are situated on the crest of a moraine that is being actively cut by the river; a period of intensified fluvial erosion of the moraine at 20–10 ka could explain the clustering of young boulder exposure ages. The sediment section at F is located close to the boulders but in a section of the moraine protruding 2–3 m above its surroundings (see Supplementary material), which, if an expression of reduced erosion at that location, could explain the older

surface exposure age. The unexpectedly young exposure ages of location A are intriguing for the incomplete exposure hypothesis because subsurface exposure accumulation during exhumation normally results in non-zero exposure ages when surfacing (cf. Heyman et al., 2011). The sharp edges of the sandstone boulders (see supplementary material) could be a result of frost shattering, potentially resulting in a significant loss in the cosmogenic exposure inventory. However, considering the nearby surface pebbles exposure age of 44.3 ± 3.8 ka to be more realistic, the required loss in inventory by frost shattering would probably be unattainable. An alternative explanation is that the boulders were rapidly exhumed a few thousand years ago. Several small lakes are located on and inside the moraine ridge (around the sampled boulders) which may have caused local abrupt moraine degradation by rapid lake drainage.

In summary, the incomplete exposure hypothesis can explain the observed exposure age disparity with reasonable assumptions. The subtle moraine ridge profiles (Fig. 6) signal substantial post-depositional degradation and the exposure age data of Qingshuihe Valley sediment sections is consistent with the interpretation that boulder and surface pebbles exposure ages are minimum limiting deglaciation ages. There is no independent chronological evidence which would substantiate cosmogenic inheritance.

Following the recommendation of Heyman et al. (2011) to interpret the oldest exposure age of each site as a minimum limiting deglaciation age, the single oldest boulder exposure age in a morphostratigraphic group becomes its minimum limiting deglaciation age (Fig. 7). For morphostratigraphic group BH-2, the extrapolated surface exposure age of the location F sediment section (93.2 ka) is slightly older than the oldest boulder exposure age of 79.9 ± 7.2 ka. However, considering the considerable geological uncertainty of sediment section exposure age interpretations in general, and the ^{10}Be concentrations of location F sediment section in particular (Table 3; Fig. 8), using the younger maximum boulder exposure age as a minimum limiting deglaciation age appears justifiable. The oldest boulder exposure age of each morphostratigraphic group is corroborated by additional exposure ages (Fig. 7). Five out of twelve boulder and surface pebbles exposure ages from group BH-1 are >43 ka. A surface pebbles exposure age of 69.9 ± 6.6 ka and a sediment section extrapolated surface exposure age of 93.2 ka of group BH-2 corroborate the 79.9 ± 7.2 ka limiting boulder exposure age for this group. Similarly, a sediment section extrapolated surface exposure age of 116.0 ka and four out of eleven boulders and surface pebbles with exposure ages >88 ka in group BH-3 corroborate the 128.7 ± 11.6 ka limiting boulder exposure age for this group. Finally, three out of eight boulders and surface pebbles in group BH-4 have exposure ages >50 ka.

6.2. Comparison of boulder, surface pebbles, and sediment section exposure ages

The exposure ages of boulder and surface pebbles differ significantly for several locations (Figs. 5 and 7), with surface pebbles exposure ages older (A, E, and F) and younger (D) than the boulder exposure ages. However, when comparing the entire dataset, boulder and surface pebbles exposure ages reveal similar patterns (cf. Briner, 2009), with oldest exposure ages of both sample types increasing from group BH-1 to BH-3 but decreasing to BH-4 (Table 4; Fig. 7). Two sediment section extrapolated surface exposure ages (F and J) are similar to the corresponding oldest boulder exposure ages of the morphostratigraphic groups whereas two sediment section extrapolated surface exposure ages (C and N) are younger than the corresponding oldest boulder exposure ages (Figs. 7 and 8). Given the wide exposure age disparity and the limited number of samples, no significant or consistent differences can be demonstrated between the exposure ages of the three sample types. An important potential advantage with the sediment section exposure ages above boulder and surface pebbles exposure ages is the possibility to quantify prior exposure of the sediments (cf. Anderson et al., 1996; Goehring et al., 2010; Hidy et al., 2010). The lowermost samples from sections F, J, and N have ^{10}Be concentrations which, assuming no shielding by the overburden, yield exposure ages of 12.0 ± 1.1 ka, 5.5 ± 0.5 ka, and 4.8 ± 0.5 ka, respectively. These low values indicate that cosmogenic inheritance is not a large component, and, thus, that the surface pebbles exposure ages in Qingshuihe Valley may be interpreted as minimum limiting deglaciation ages.

The data further usefully illustrates the importance of collecting multiple sample types. If, for example, only boulders had been sampled and dated in Qingshuihe Valley (Figs. 5 and 7), the resulting age inferences would have been significantly different.

6.3. Comparison with boulder exposure ages from surrounding regions

The Bayan Har Shan exposure ages add chronological constraints for past glaciation of the northeastern Tibetan Plateau. The exposure ages are consistent with previously reported exposure ages from other regions of the central and eastern Tibetan Plateau (Fig. 10; Owen et al., 2008; Heyman et al., 2011). West of Bayan Har Shan, in more central and dryer areas of the plateau, exposure ages ranging up to 194 ka and 218 ka (Heyman et al., 2011) have been reported from the Tanggula Shan (Schäfer et al., 2002; Owen et al., 2005; Colgan et al., 2006) and the Kunlun Pass (Owen et al., 2006b), respectively. East of Bayan Har Shan, in steeper and wetter areas affected more by monsoon precipitation, exposure ages ranging up to 49 ka, 66 ka, and 63 ka (Heyman et al., 2011) have been reported from the Anyemaqen Shan, the Nianbaoyeze Shan, and the La Ji Shan, respectively (Owen et al.,

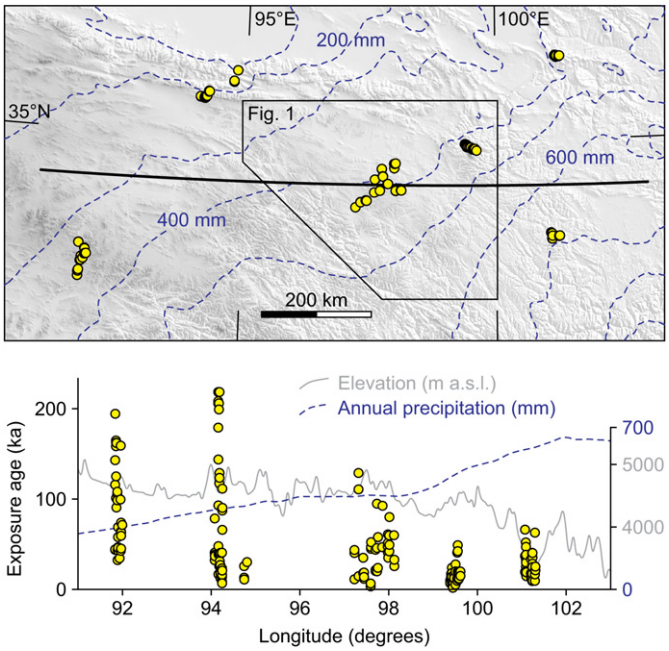

Fig. 10. Boulder exposure ages (Heyman et al., 2011), elevation data (Jarvis et al., 2008), and annual precipitation (Hijmans et al., 2005) for the northeastern Tibetan Plateau. Maximum exposure ages decrease towards the plateau margin in the east where topographic relief and annual precipitation totals increase.

Fig. 11. Frontal moraine in the centre of Bayan Har Shan. The moraine ridge is located at c. 4800 m a.s.l. and was formed by a small (c. 1 km long) cirque glacier subsequent to BH-1. See Fig. 5 for location.

2003a,b). Bayan Har Shan, located in-between these areas, yield intermediate boulder exposure ages ranging up to 129 ka. The location – exposure age relationship (Fig. 10), with maximum exposure ages getting younger towards the eastern plateau margin, may reflect two factors. First, glaciers in the eastern areas may have advanced further during MIS-3 to MIS-2, controlled by increased precipitation (cf. Owen et al., 2003a, 2005, 2008), thus erasing glacial deposits formed by earlier glaciations. Second, the steeper relief and higher precipitation quantities along the eastern margin may have caused more intense landform degradation to occur, with traces of older and more extensive glaciations, which are still present in the central areas, having been erased (cf. Schaefer et al., 2008; Stroeven et al., 2009; Craddock et al., 2010).

An interesting result is that the moraines formed by the most restricted glaciers in central Bayan Har Shan (morphostratigraphic group BH-1) have exposure ages older than exposure ages from moraines in the Anyemaqen Shan that occur up to 12 km away from the present-day ice margin (Owen et al., 2003a; Heyman et al., 2011). Results of the glacier model (Fig. 9) show that the climate forcing required to form any glaciers at all in central Bayan Har Shan will simultaneously allow glaciers in the Anyemaqen Shan to expand well beyond the moraines dated to MIS-2 and the late Holocene by Owen et al. (2003a). This is valid for both required temperature (−3 K) and precipitation (1200%) perturbations. Thus, the model lends further support to the conclusion that glaciers in Bayan Har Shan have remained highly restricted over at least the last 40 ka.

Up-valley of location D, just below the highest peaks of central Bayan Har Shan, a moraine ridge marks the extent of a former small cirque glacier (Figs. 5 and 11). This moraine is too small to be resolved in the employed Landsat satellite imagery or the SRTM elevation data and it has not been mapped (cf. Heyman et al., 2008). The moraine indicates that small glaciers developed in the highest part of central Bayan Har Shan subsequent to the BH-1 glaciation (minimum age of 40–65 ka), and, arguably speculatively, this may be the faint expression of ice expansion during the LGM in the Bayan Har Shan.

6.4. Palaeoglaciological reconstruction

Based on presented ^{10}Be exposure ages, glacier modelling, and previous studies of the glacial geomorphology and surface stratigraphy (Heyman et al., 2008, 2009; Stroeven et al., 2009), we present a time-slice reconstruction of past glacial extent in the Bayan Har Shan (Fig. 12). We assign age spans to each spatial reconstruction based on minimum deglaciation ages for the various CRONUS ^{10}Be production rate scaling schemes and their uncertainties (Tables 2 and 4; Balco et al., 2008). The most restricted glaciation of central Bayan Har Shan (morphostratigraphic group BH-1), with glaciers shorter than 10 km, dates to at least 40–65 ka (based on TB-07-92). Two older glacial extents, BH-2 and BH-3, with glacier margins 30–60 km distanced from the highest mountains, date to at least 60–100 ka (based on TB-06-48) and at least 95–165 ka (based on TB-07-40), respectively. The age of the largest glacial extent (BH-4; Heyman et al., 2009) remains elusive. Based on morphostratigraphy, group BH-4 should pre-date BH-3 and is therefore assigned the same minimum age span of 95–165 ka as BH-3.

The central Bayan Har Shan exposure ages do not allow an exact determination of the timing of past glaciations. However, they do clearly demonstrate that over the LGM glaciers have remained highly restricted or were absent. The BH-1 moraines, with a minimum age of 40–65 ka, were formed by glaciers similar in size to the present-day Tanggula Shan glaciers on the central Tibetan Plateau (cf. Morén et al., 2011). The old age of this highly restricted glacial extent is remarkable considering the evidence of extensive ice field/ice cap glaciation in the area (Heyman et al., 2009) and implies that the glacial geomorphology in Bayan Har Shan is predominantly a relict imprint pre-dating MIS-3.

The Bayan Har Shan reconstruction is the first of its kind for the Tibetan Plateau, integrating different strands of evidence for a larger region of its northeastern sector. Similar to several other sites on the Tibetan Plateau (e.g. Schäfer et al., 2002; Finkel et al., 2003; Mériaux et al., 2004; Owen et al., 2005, 2006a, 2006b,

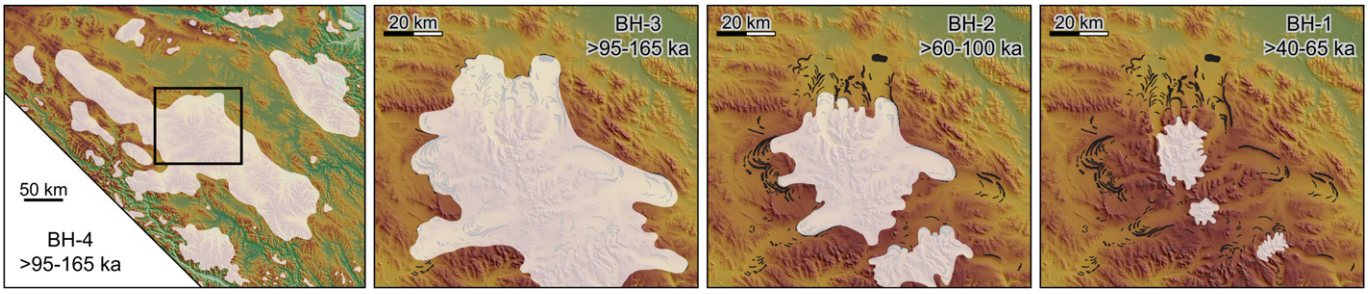

Fig. 12. Time-slice reconstruction for central Bayan Har Shan. The given time spans are based on the exposure ages of the oldest boulder (cf. Heyman et al., 2011) in the morphostratigraphic groups BH-1 to BH-3 (Fig. 7) and include the variations of the different production rate scaling schemes (Balco et al., 2008; Supplementary material). The time spans indicate minimum ages for the four mapped glacial extents. The outline of BH-4 for the entire Bayan Har Shan study area is based on the glacial traces presented in Heyman et al. (2009). The central Bayan Har Shan glacier outlines for BH-1 to BH-3 are tentative spatial reconstructions based on moraine morphology and assumed topographic steering of ice. The largest ice mass of the BH-4 reconstruction is c. 26 000 km^2, slightly larger than the two present-day Patagonian ice fields together. The reconstructed BH-3 and BH-2 glaciers are c. 4600 km^2 and 2200 km^2, respectively, similar in size to half Vatnajökull and half Barnes ice cap. The reconstructed BH-1 glaciers cover c. 400 km^2, and are similar in size to the present-day Tanggula Shan ice fields.

2009, 2010; Zech et al., 2005; Schaefer et al., 2008; Seong et al., 2009; Dortch et al., 2010; Chevalier et al., 2011; Hedrick et al., 2011; Heyman et al., 2011) exposure ages from the Bayan Har Shan show that glaciers on the Tibetan Plateau behaved entirely differently from glaciers and ice sheets in North America and Scandinavia during the second half of the last glacial cycle.

7. Conclusions

Exposure dating of glacial deposits, in conjunction with mapping of glacial geomorphology using remote sensing, field studies of surface stratigraphy, and glacier modelling allow us to draw the following conclusions on past glaciations in Bayan Har Shan on the northeastern Tibetan Plateau;

- Samples from glacial boulders, surface pebbles and sediment sections in central Bayan Har Shan yield exposure ages exhibiting a large disparity. No significant or consistent exposure age differences between the three sample types can be demonstrated with this dataset. Sediment section cosmogenic exposure ages allow evaluation of cosmogenic inheritance of the sediments.
- The youngest glaciation of central Bayan Har Shan, with glaciers less than 10 km long, has a minimum age of 40–65 ka. Two older and significantly more extensive glaciations have minimum ages of 60–100 ka and 95–165 ka. The timing of the maximum glacial extent is still elusive, but should pre-date the 95–165 ka glaciation. The vast majority of the Bayan Har Shan glacial traces were therefore formed prior to MIS-3, which highlights a notable absence of an LGM expansion.
- The palaeoglaciology of Bayan Har Shan involves multiple stages of alpine glacier and ice field/ice cap expansion and retreat. During the global LGM, glaciers in Bayan Har Shan were either absent or very small. This verifies limited Tibetan glaciation during the global LGM, and raises important questions about palaeoclimate and glacier dynamics on the Tibetan Plateau.

Acknowledgements

We thank Dong Jianyi, Liu Feng, Ma Luyi, Martin Machiedo and Daniel Veres for fieldwork assistance, Susan Ma for ^{10}Be calculations, and Patrick Applegate for helpful comments that improved the manuscript. We thank Lewis Owen and an anonymous reviewer for constructive reviews. Funding for this study was provided by the Swedish Research Council/Swedish International Development Cooperation Agency (VR/SIDA) through their Swedish Research Links programme to Stroeven (No. 348-2004-5684 and 348-2007-6924) and by the Swedish Society for Anthropology and Geography, the Royal Swedish Academy of Sciences, Helge Ax:son Johnsons stiftelse, Carl Mannerfelts fond, August Emil Wilhelm Smitts stipendiestiftelse, and the Bert Bolin Centre for Climate Research to Heyman.

Appendix. Supplementary material

Supplementary data associated with this article can be found, in the online version, at doi:10.1016/j.quascirev.2011.05.002.

References

An, Z.S., Kutzbach, J.E., Prell, W.L., Porter, S.C., 2001. Evolution of Asian monsoons and phased uplift of the Himalaya-Tibetan plateau since late Miocene times. Nature 411, 62–66.

Anderson, R.S., Repka, J.L., Dick, G.S., 1996. Explicit treatment of inheritance in dating depositional surfaces using in situ ^{10}Be and ^{26}Al. Geology 24, 47–51.

Applegate, P.J., Urban, N.M., Laabs, B.J.C., Keller, K., Alley, R.B., 2010. Modeling the statistical distributions of cosmogenic exposure dates from moraines. Geoscientific Model Development 3, 293–307.

Balco, G., Stone, J.O., Lifton, N.A., Dunai, T.J., 2008. A complete and easily accessible means of calculating surface exposure ages or erosion rates from ^{10}Be and ^{26}Al measurements. Quaternary Geochronology 3, 174–195.

Barr, I.D., 2009. Constraining the extent, style and phases of glaciation to derive late Quaternary equilibrium-line altitude estimates in far NE Russia. PhD Thesis, University of Sheffield.

Braithwaite, R.J., 2008. Temperature and precipitation climate at the equilibrium-line altitude of glaciers expressed by the degree-day factor for melting snow. Journal of Glaciology 54, 437–444.

Briner, J.P., 2009. Moraine pebbles and boulders yield indistinguishable ^{10}Be ages: a case study from Colorado, USA. Quaternary Geochronology 4, 299–305.

Briner, J.P., Kaufman, D.S., Manley, W.F., Finkel, R.C., Caffee, M.W., 2005. Cosmogenic exposure dating of late Pleistocene moraine stabilization in Alaska. Geological Society of America Bulletin 117, 1108–1120.

Chamberlin, T.C., 1890. The method of multiple working hypotheses. Science 15, 92–96.

Cheng, J., Zhang, X.J., Tian, M.Z., Yu, W.Y., Yu, J.K., 2005. Ice-wedge casts showing climatic change since the late Pleistocene in the source area of the Yellow River, northeast Tibet. Journal of Mountain Science 2, 193–201.

Chevalier, M.-L., Hilley, G., Tapponnier, P., Van der Woerd, J., Jing, L.Z., Finkel, R.C., Ryerson, F.J., Li, H.B., Liu, X.H., 2011. Constraints on the late Quaternary glaciations in Tibet from cosmogenic exposure ages of moraine surfaces. Quaternary Science Reviews 30, 528–554.

Chmeleff, J., von Blanckenburg, F., Kossert, K., Jakob, D., 2010. Determination of the ^{10}Be half-life by multicollector ICP-MS and liquid scintillation counting. Nuclear Instruments and Methods in Physics Research B 268, 192–199.

Clark, P.U., Dyke, A.S., Shakun, J.D., Carlson, A.E., Clark, J., Wohlfarth, B., Mitrovica, J.X., Hostetler, S.W., McCabe, A.M., 2009. The last glacial maximum. Science 325, 710–714.

Colgan, P.M., Munroe, J.S., Zhou, S.Z., 2006. Cosmogenic radionuclide evidence for the limited extent of last glacial maximum glaciers in the Tanggula Shan of the central Tibetan plateau. Quaternary Research 65, 336–339.

Craddock, W.H., Kirby, E., Harkins, N.W., Zhang, H.P., Shi, X.H., Liu, J.H., 2010. Rapid fluvial incision along the Yellow River during headward basin integration. Nature Geoscience 3, 209–213.

Derbyshire, E., Shi, Y.F., Li, J.J., Zheng, B.X., Li, S.J., Wang, J.T., 1991. Quaternary glaciation of Tibet: the geological evidence. Quaternary Science Reviews 10, 485–510.

Dortch, J.M., Owen, L.A., Caffee, M.W., 2010. Quaternary glaciation in the Nubra and Shyok valley confluence, northernmost Ladakh, India. Quaternary Research 74, 132–144.

Dyurgerov, M.B., Meier, M.F., 2005. Glaciers and the Changing Earth System: A 2004 Snapshot. INSTAAR Occasional Paper 58. Institute of Arctic and Alpine Research, University of Colorado, USA.

Fabel, D., Fink, D., Fredin, O., Harbor, J., Land, M., Stroeven, A.P., 2006. Exposure ages from relict lateral moraines overridden by the Fennoscandian ice sheet. Quaternary Research 65, 136–146.

Finkel, R.C., Owen, L.A., Barnard, P.L., Caffee, M.W., 2003. Beryllium-10 dating of Mount Everest moraines indicates a strong monsoon influence and glacial synchroneity throughout the Himalaya. Geology 31, 561–564.

Fredin, O., Hättestrand, C., 2002. Relict lateral moraines in northern Sweden – evidence for an early mountain centred ice sheet. Sedimentary Geology 149, 145–156.

Goehring, B.M., Kelly, M.A., Schaefer, J.M., Finkel, R.C., Lowell, T.V., 2010. Dating of raised marine and lacustrine deposits in east Greenland using beryllium-10 depth profiles and implications for estimates of subglacial erosion. Journal of Quaternary Science 25, 865–874.

Goodfellow, B.W., 2007. Relict non-glacial surfaces in formerly glaciated landscapes. Earth-Science Reviews 80, 47–73.

Gosse, J.C., Phillips, F.M., 2001. Terrestrial in situ cosmogenic nuclides: theory and application. Quaternary Science Reviews 20, 1475–1560.

Granger, D.E., Smith, A.L., 2000. Dating buried sediments using radioactive decay and muogenic production of ^{26}Al and ^{10}Be. Nuclear Instruments and Methods in Physics Research B 172, 822–826.

Hallet, B., Putkonen, J., 1994. Surface dating of dynamic landforms: young boulders on aging moraines. Science 265, 937–940.

Hättestrand, C., Kolka, V., Stroeven, A.P., 2007. The Keiva ice marginal zone on the Kola Peninsula, northwest Russia: a key component for reconstructing the palaeoglaciology of the northeastern Fennoscandian ice sheet. Boreas 36, 352–370.

Hedrick, K.A., Seong, Y.B., Owen, L.A., Caffee, M.W., Dietsch, C., 2011. Towards defining the transition in style and timing of Quaternary glaciation between the monsoon-influenced greater Himalaya and the semi-arid Transhimalaya of Northern India. Quaternary International 236, 21–33.

Heyman, J., Hättestrand, C., Stroeven, A.P., 2008. Glacial geomorphology of the Bayan Har sector of the NE Tibetan plateau. Journal of Maps 2008, 42–62.

Heyman, J., Stroeven, A.P., Alexanderson, H., Hättestrand, C., Harbor, J., Li, Y.K., Caffee, M.W., Zhou, L.P., Veres, D., Liu, F., Machiedo, M., 2009. Palaeoglaciation of Bayan Har Shan, northeastern Tibetan Plateau: glacial geology indicates maximum extents limited to ice cap and ice field scales. Journal of Quaternary Science 24, 710–727.

Heyman, J., Stroeven, A.P., Harbor, J., Caffee, M.W., 2011. Too young or too old: evaluating cosmogenic exposure dating based on an analysis of compiled boulder exposure ages. Earth and Planetary Science Letters 302, 71–80.
Hidy, A.J., Gosse, J.C., Pederson, J.L., Mattern, J.P., Finkel, R.C., 2010. A geologically constrained Monte Carlo approach to modeling exposure ages from profiles of cosmogenic nuclides: an example from Lees Ferry, Arizona. Geochemistry, Geophysics, Geosystems 11, Q0AA10.
Hijmans, R.J., Cameron, S.E., Parra, J.L., Jones, P.G., Jarvis, A., 2005. Very high resolution interpolated climate surfaces for global land areas. International Journal of Climatology 25, 1965–1978.
Huang, C.K., Ye, T.Z., Chen, K.Q., Wu, K.L., Ji, X.Y., Gao, Z.J., Qian, D.D., Tian, Y.Y., He, Y.X., Zhang, Q.H., Cao, B.G., Li, L., Shao, H.M., Wang, Y.Q., Yang, M.G., Zhang, Z.W., Yao, D.S., Zheng, J.K., 2004. Geological Map of the People's Republic of China. SinoMaps Press, Xian.
Hubbard, A., 1999. High-resolution modeling of the advance of the Younger Dryas ice sheet and its climate in Scotland. Quaternary Research 52, 27–43.
Hubbard, A., 2000. The verification and significance of three approaches to longitudinal stresses in high-resolution models of glacier flow. Geografiska Annaler 82A, 471–487.
Hubbard, A., Blatter, H., Nienow, P., Mair, D., Hubbard, B., 1998. Comparison of a three-dimensional model for glacier flow with field data from Haut Glacier d'Arolla, Switzerland. Journal of Glaciology 44, 368–378.
Jarvis, A., Reuter, H.I., Nelson, A., Guevara, E., 2008. Hole-filled seamless SRTM data V4. International Centre for Tropical Agriculture (CIAT). Available from. http://srtm.csi.cgiar.org.
Kleman, J., 1992. The palimpsest glacial landscape in northwestern Sweden. Geografiska Annaler 74A, 305–325.
Kleman, J., 1994. Preservation of landforms under ice sheets and ice caps. Geomorphology 9, 19–32.
Kleman, J., Hättestrand, C., 1999. Frozen-bed Fennoscandian and Laurentide ice sheets during the last glacial maximum. Nature 402, 63–66.
Kleman, J., Stroeven, A.P., 1997. Preglacial surface remnants and Quaternary glacial regimes in northwestern Sweden. Geomorphology 19, 35–54.
Kohl, C.P., Nishiizumi, K., 1992. Chemical isolation of quartz for measurement of in-situ-produced cosmogenic nuclides. Geochimica et Cosmochimica Acta 56, 3586–3587.
Korschinek, G., Bergmaier, A., Faestermann, T., Gerstmann, U.C., Knie, K., Rugel, G., Wallner, A., Dillmann, I., Dollinger, G., von Gostomski, C.L., Kossert, K., Maiti, M., Poutivtsev, M., Remmert, A., 2010. A new value for the half-life of ^{10}Be by heavy-ion elastic recoil detection and liquid scintillation counting. Nuclear Instruments and Methods in Physics Research B 268, 187–191.
Kuhle, M., 2004. The high glacial (last ice age and LGM) ice cover in high and central Asia. In: Ehlers, J., Gibbard, P.L. (Eds.), Quaternary Glaciations – Extent and Chronology, Part III: South America, Asia, Africa, Australia, Antarctica. Elsevier, Amsterdam, pp. 175–199.
Lal, D., 1991. Cosmic ray labeling of erosion surfaces: in situ nuclide production rates and erosion models. Earth and Planetary Science Letters 104, 424–439.
Lehmkuhl, F., Owen, L.A., 2005. Late Quaternary glaciation of Tibet and the bordering mountains: a review. Boreas 34, 87–100.
Lehmkuhl, F., Owen, L.A., Derbyshire, E., 1998. Late Quaternary glacial history of northeast Tibet. Quaternary Proceedings 6, 121–142.
Li, B.Y., Li, J.J., Cui, Z.J., Zheng, B.X., Zhang, Q.S., Wang, F.B., Zhou, S.Z., Shi, Z.H., Jiao, K.Q., Kang, J.C., 1991. Quaternary Glacial Distribution Map of Qinghai-Xizang (Tibet) Plateau. Science Press, Beijing.
Mériaux, A.-S., Ryerson, F.J., Tapponnier, P., Van der Woerd, J., Finkel, R.C., Xu, X.W., Xu, Z.Q., Caffee, M.W., 2004. Rapid slip along the central Altyn Tagh Fault: morphochronologic evidence from Cherchen He and Sulamu Tagh. Journal of Geophysical Research 109, B06401.
Morén, B., Heyman, J., Stroeven, A.P., 2011. Glacial geomorphology of the central Tibetan Plateau. Journal of Maps 2011, 115–125.
Nelder, J.A., Mead, R., 1965. A simplex method for function minimization. Computer Journal 7, 308–313.
Nishiizumi, K., Winterer, E., Kohl, C., Klein, J., Middleton, R., Lal, D., Arnold, J., 1989. Cosmic ray production rates of ^{26}Al and ^{10}Be in quartz from glacially polished rocks. Journal of Geophysical Research 94, 17907–17915.
Nishiizumi, K., Imamura, M., Caffee, M.W., Southon, J.R., Finkel, R.C., McAninch, J., 2007. Absolute calibration of ^{10}Be AMS standards. Nuclear Instruments and Methods in Physics Research B 258, 403–413.
Owen, L.A., Finkel, R.C., Ma, H.Z., Spencer, J.Q., Derbyshire, E., Barnard, P.L., Caffee, M.W., 2003a. Timing and style of Late Quaternary glaciation in northeastern Tibet. Geological Society of America Bulletin 115, 1356–1364.
Owen, L.A., Ma, H.Z., Derbyshire, E., Spencer, J.Q., Barnard, P.L., Zeng, Y.N., Finkel, R.C., Caffee, M.W., 2003b. The timing and style of late Quaternary glaciation in the La Ji Mountains, NE Tibet: evidence for restricted glaciation during the latter part of the last glacial. Zeitschrift für Geomorphologie NF Supplementband 130, 263–276.
Owen, L.A., Finkel, R.C., Barnard, P.L., Ma, H.Z., Asahi, K., Caffee, M.W., Derbyshire, E., 2005. Climatic and topographic controls on the style and timing of late Quaternary glaciation throughout Tibet and the Himalaya defined by ^{10}Be cosmogenic radionuclide surface exposure dating. Quaternary Science Reviews 24, 1391–1411.
Owen, L.A., Caffee, M.W., Bovard, K.R., Finkel, R.C., Sharma, M.C., 2006a. Terrestrial cosmogenic nuclide surface exposure dating of the oldest glacial successions in the Himalayan orogen: Ladakh Range, northern India. Geological Society of America Bulletin 118, 383–392.
Owen, L.A., Finkel, R.C., Ma, H.Z., Barnard, P.L., 2006b. Late Quaternary landscape evolution in the Kunlun mountains and Qaidam basin, northern Tibet: a framework for examining the links between glaciation, lake level changes and alluvial fan formation. Quaternary International 154-155, 73–86.
Owen, L.A., Caffee, M.W., Finkel, R.C., Seong, Y.B., 2008. Quaternary glaciation of the Himalayan-Tibetan orogen. Journal of Quaternary Science 23, 513–531.
Owen, L.A., Robinson, R., Benn, D.I., Finkel, R.C., Davis, N.K., Yi, C.L., Putkonen, J., Li, D.W., Murray, A.S., 2009. Quaternary glaciation of Mount Everest. Quaternary Science Reviews 28, 1412–1433.
Owen, L.A., Yi, C.L., Finkel, R.C., Davis, N.K., 2010. Quaternary glaciation of Gurla Mandhata (Naimon'anyi). Quaternary Science Reviews 29, 1817–1830.
Putkonen, J., Swanson, T., 2003. Accuracy of cosmogenic ages for moraines. Quaternary Research 59, 255–261.
Putkonen, J., Connolly, J., Orloff, T., 2008. Landscape evolution degrades the geologic signature of past glaciations. Geomorphology 97, 208–217.
Raymo, M.E., Ruddiman, W.F., 1992. Tectonic forcing of late Cenozoic climate. Nature 359, 117–122.
Richards, B.W.M., 2000. Luminescence dating of Quaternary sediments in the Himalaya and high Asia: a practical guide to its use and limitations for constraining the timing of glaciation. Quaternary International 65/66, 49–61.
Rodés, Á, Pallàs, R., Braucher, R., Moreno, X., Masana, E., Bourlés, D.L., 2011. Effect of density uncertainties in cosmogenic ^{10}Be depth-profiles: dating a cemented Pleistocene alluvial fan (Carboneras Fault, SE Iberia). Quaternary Geochronology 6, 186–194.
Rutter, N., 1995. Problematic ice sheets. Quaternary International 28, 19–37.
Schaefer, J.M., Oberholzer, P., Zhao, Z.Z., Ivy-Ochs, S., Wieler, R., Baur, H., Kubik, P.W., Schlüchter, C., 2008. Cosmogenic beryllium-10 and neon-21 dating of late Pleistocene glaciations in Nyalam, monsoonal Himalayas. Quaternary Science Reviews 27, 295–311.
Schäfer, J.M., Tschudi, S., Zhao, Z.Z., Wu, X.H., Ivy-Ochs, S., Wieler, R., Baur, H., Kubik, P.W., Schlüchter, C., 2002. The limited influence of glaciations in Tibet on global climate over the past 1 70 000 yr. Earth and Planetary Science Letters 194, 287–297.
Seong, Y.B., Owen, L.A., Yi, C.L., Finkel, R.C., 2009. Quaternary glaciation of Muztag Ata and Kongur Shan: evidence for glacier response to rapid climate changes throughout the late glacial and Holocene in westernmost Tibet. Geolocial Society of America Bulletin 121, 348–365.
Stone, J.O., 2000. Air pressure and cosmogenic isotope production. Journal of Geophysical Research 105 (B10), 23753–23759.
Stroeven, A.P., Hättestrand, C., Heyman, J., Harbor, J., Li, Y.K., Zhou, L.P., Caffee, M.W., Alexanderson, H., Kleman, J., Ma, H.Z., Liu, G.N., 2009. Landscape analysis of the Huang He headwaters, NE Tibetan Plateau – patterns of glacial and fluvial erosion. Geomorphology 103, 212–226.
Wang, J.T., 1987. Climatic geomorphology of the northeastern part of the Qinghai-Xizang Plateau. In: Hövermann, J., Wang, W.Y. (Eds.), Reports on the Northeastern Part of the Qinghai-Xizang (Tibet) Plateau. Science Press, Beijing, pp. 140–175.
Yi, C.L., Zhu, Z.Y., Wei, L., Cui, Z.J., Zheng, B.X., Shi, Y.F., 2007. Advances in numerical dating of Quaternary glaciations in China. Zeitschrift für Geomorphologie 51 (Suppl. 2), 153–175.
Zech, R., Abramowski, U., Glaser, B., Sosin, P., Kubik, P.W., Zech, W., 2005. Late Quaternary glacial and climate history of the Pamir Mountains derived from cosmogenic ^{10}Be exposure ages. Quaternary Research 64, 212–220.
Zheng, B.X., Rutter, N., 1998. On the problem of Quaternary glaciations, and the extent and patterns of Pleistocene ice cover in the Qinghai-Xizang (Tibet) Plateau. Quaternary International 45/46, 109–122.
Zhou, S.Z., Li, J.J., 1998. The sequence of Quaternary glaciation in the Bayan Har mountains. Quaternary International 45/46, 135–142.
Zhou, S.Z., Li, J.J., Zhang, S.Q., Zhao, J.D., Cui, J.X., 2004. Quaternary glaciations in China. In: Ehlers, J., Gibbard, P.L. (Eds.), Quaternary Glaciations - Extent and Chronology, Part III: South America, Asia, Africa, Australia, Antarctica. Elsevier, Amsterdam, pp. 105–113.
Zreda, M.G., Phillips, F.M., Elmore, D., 1994. Cosmogenic ^{36}Cl accumulation in unstable landforms 2. Simulations and measurements on eroding moraines. Water Resources Research 30, 3127–3136.